NRMRL-RTP-P-185

EPA/600/A-97/022

LOSS MODELING OF CONVERTER INDUCTION MACHINE SYSTEM FOR VARIABLE SPEED DRIVE*

Gilberto C. D. Sousa**, Bimal K. Bose
Department of Electrical Engineering
The University of Tennessee
Knoxville, TN 37996

John Cleland
Research Triangle Institute
Research Triangle Park, NC 27709

Ronald J. Spiegel and P. Jeffrey Chappell
US Environmental Protection Agency
Air & Energy Engineering Research Laboratory
Research Triangle Park, NC 27711

ABSTRACT

A reliable and reasonably accurate loss model of a converter induction machine system is extremely important for performance prediction of variable speed drive. The paper describes a unified loss model development of converter machine system such that steady state loss characteristics as well as the dynamic behavior of both machine and converter are accurately represented in the model. The machine electrical losses, such as stator and rotor copper loss, core loss, and stray loss are considered for both fundamental and harmonic frequencies. Also considered are the skin effect on rotor resistance, temperature effect on both stator and rotor resistances, magnetizing inductance saturation, and friction and windage loss. All the above features are incorporated in a synchronously rotating frame dynamic D^e-Q^e equivalent circuits. A converter system that includes a diode rectifier and PWM transistor inverter has been modeled accurately for conduction and switching losses. The machine and converter models have been simulated for a vector controlled drive system and validity in both steady state and transient condition has been verified. The models are valid for any type of control strategy with an arbitrary PWM algorithm, and can be used for purposes, such as loss-optimized design of converter machine system, efficiency evaluation, cooling system design and general dynamic studies.

1. INTRODUCTION

Precise and reliable loss models for induction motor and converter systems are very important for performance prediction of variable speed drives. The machine electrical losses, such as copper loss, core loss and stray load loss have been traditionally studied by using per-phase equivalent circuit because the losses become primarily important in steady state condition. However, the same equivalent circuit can not be used in transient condition. On the other hand, for dynamic study, the synchronously rotating D^e-Q^e model is normally used, but in this case the losses are not properly represented. With sinusoidal power supply, precise evaluation of machine losses is not straightforward. With inverter-fed power supply that generates harmonic-rich non-sinusoidal waveforms, the machine loss model becomes much more complex. Loss modeling of induction motor has received wide attention in the literature over a number of years. Neglecting the effects of space harmonics, the machine parameters become dependent of time harmonic frequencies impressed by the inverter. Klingshim and Jordan [6] applied superposition principle to calculate harmonic currents and the corresponding losses with per-phase equivalent circuit, where the rotor resistance and leakage inductance for each harmonic were corrected for deep bar (skin) effect. Kawagishi et al. [7] were able to verify experimentally the frequency dependency of parameter by using a high frequency power supply and validate some of the theoretical predictions. Honsinger [1] systematically studied the losses for a six-step inverter-fed machine and propose harmonic per-phase equivalent circuit. Since both core loss and stray load loss are basically due to hysteresis and eddy current effects, he proposed representation of stray loss by frequency dependent resistance in parallel with leakage inductance in the equivalent circuit. More recently, Udayagiri and Lipo [3] proposed a new simulation model that incorporates core loss but neglects the skin effect and leakage flux induced core loss, thereby underestimating the total loss.

In high frequency PWM inverter system, both conduction loss and switching loss are important in the loss model. The switching loss has been discussed analytically by McMurray [8] where the effect of both turn-on and turn-off snubbers was considered. Jovanovich et al. [9] made experimental evaluation of switching characteristics and losses for a number of power devices with different base drives and load conditions. Ikeda et al. [10] have proposed loss modeling of PWM voltage-fed inverter and discussed the effect of carrier frequency on inverter losses. Circuit simulation programs, such as PSPICE that embed the detailed model of devices can give realistic lossy converter simulation. However, the drawbacks are that the losses remain somewhat transparent and can not be easily partitioned between the conduction and switching losses. Besides, such programs are not convenient for drive system simulation.

In this paper, both induction motor and PWM converter system lossy models have been derived in detail for variable frequency drive system shown in Fig. 1, and then validated by extensive simulation study. The unified system loss model can be used for both transient and steady state performance evaluation. The motivation for the project is to predict losses in a vector-controlled motor drive that uses fuzzy logic based efficiency optimization control.

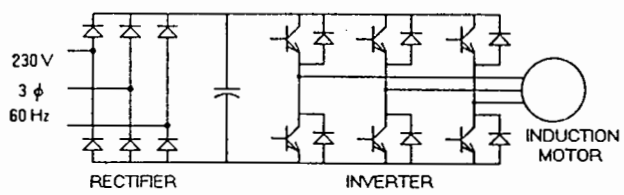

Fig. 1. Converter-machine system for variable speed drive.

* The project was funded in part by the US Environmental Protection Agency under the subcontract from Research Triangle Institute.

** Mr. Sousa is a member of faculty in the Federal University of Espirito Santo, Brazil, and is currently pursuing doctoral study in the University of Tennessee.

0-7803-0582-5 /92$3.00©1992 IEEE

2. LOSS MODELING OF INDUCTION MACHINE

2.1. Electrical and Mechanical Losses

Copper Loss

Proper evaluation of copper loss requires the consideration of temperature (discussed in the next subsection) and skin effect on winding resistance. The skin effect in stator winding in lower end of power rating can be ignored, but the effect is very dominant in rotor bars of squirrel cage machine. The skin effect has been widely discussed in the literature. In inverter-fed machine, the skin effect due to fundamental slip frequency can be ignored, but for the harmonic frequencies the rotor appears almost stationary, and therefore, practically all the stator harmonic currents flow in the rotor creating dominant skin effect. The rotor resistance at harmonic frequency f_n is given approximately by [5]

$$R_{rn} = R_{rdc}\ (1 + c_1\ d\ f_n^{0.5}) \tag{1}$$

where R_{rdc} = dc resistance, d = bar depth, and c_1 is a constant that takes into account the bar material and shape. With a number of harmonic frequencies, the superposition principle can be applied approximately by assuming that machine parameters for all harmonic frequencies are identical to those computed at carrier frequency. For a PWM inverter with sinusoidal PWM or hysteresis-band current control, the carrier frequency and the near sidebands are most dominant.

Core Losses

A precise prediction of core losses associated with high frequency harmonic fluxes is a very difficult task [4]. Here, it is assumed that the core losses due to mutual harmonic flux are governed by the same principle that controls the losses by fundamental mutual flux. The stator core loss P_{cs} due to fundamental frequency mutual flux ϕ can be given as

$$P_{cs} = k_h\ f\ \phi^2 + k_e\ f^2\ \phi^2 \tag{2}$$

where f is the fundamental frequency, and k_h and k_e are the hysteresis and eddy current coefficients, respectively. The corresponding rotor core loss is given as

$$P_{cr} = k_h\ s\ f\ \phi^2 + k_e\ (s\ f)^2\ \phi^2 \tag{3}$$

here f is substituted by s f (s = per unit slip). These equations can be added and rearranged as follows:

$$P_c = P_{cs} + P_{cr} = [k_h \frac{(1+s)}{f} + k_e(1+s^2)] f^2 \phi^2 \tag{4}$$

As the mutual or air-gap flux ϕ is related to air-gap voltage V_m by

$$\phi = \sqrt{k_c}\ \frac{V_m}{f} \tag{5}$$

eqn. 4 can be rewritten as

$$P_c = k_c\ [k_h\ \frac{(1+s)}{f} + k_e(1+s^2)]\ V_m^2 \tag{6}$$

The equivalent core loss resistance R_m can then be derived as

$$R_m = \frac{1}{k_c[k_h \frac{(1+s)}{f} + k_e(1+s^2)]} \tag{7}$$

Assuming that the coefficients k_h and k_e remain the same at harmonic frequency, and since harmonic slip $s_n \approx 1$ the equivalent core loss resistance R_{mn} at frequency f_n can be obtained from eqn. 7 as

$$R_{mn} = \frac{0.5}{k_c[\frac{k_h}{f_n} + k_e]} \tag{8}$$

Stray Losses

The stray losses actually represent a group of losses, as indicated by Alger et al. [11]. They used empirical equations to evaluate each individual loss component that requires the knowledge of machine dimensions, type of core material, lamination thickness, winding geometry, etc. In this work, however, instead of evaluating stray loss individually, we treat them as a whole. The fundamental idea is that the stray loss is essentially due to eddy current and hysteresis losses induced by various types of leakage fluxes in the laminations and other structural parts of the machine. Therefore, the stray loss can be modeled in a way similar to that used for core loss modeling. The stator per phase stray loss at harmonic frequency f_n can be given as

$$P_{sln} = k_{sln}[\frac{k_n}{f_n} + k_e]\ V_{sln}^2 \tag{9}$$

where V_{sln} = voltage across the stator leakage inductance and k_{sln} = stray loss constant. The loss can be represented by an equivalent resistance R_{sln} in parallel with the leakage inductance as

$$R_{sln} = \frac{1}{k_{sln}[\frac{k_h}{f_n} + k_e]} \tag{10}$$

A similar expression can be derived for rotor harmonic stray loss. The stray loss due to fundamental current is essentially concentrated in the stator and an equation similar to eqn. 10 can also be used. However, this resistance will be represented in series with the stator leakage reactance X_{ls} for reasons that will be clear later. The fundamental voltage drop V_{sl1} across the leakage reactance X_{ls} is $2\pi\ f\ L_{ls}\ I_{s1}$, where I_{s1} is the fundamental stator current. It can be substituted in eqn. 9 to derive fundamental per-phase stray loss P_{sl1} as

$$P_{sl1} = k_{sl1}\ [k_h f + k_e f^2]\ I_{s1}^2 = R_{sl1}\ I_{s1}^2 \tag{11}$$

where R_{sl1} = equivalent series resistance (see Fig. 2(c)). From this expression, R_{sl1} is given as

$$R_{sl1} = k_{sl1}\ [k_h f + k_e f^2] \tag{12}$$

Friction and windage losses

The friction and windage loss is essentially a function of motor speed w_r and does not depend on the type of power supply. It can be expressed as

$$P_{fw} = k_{fw}\ w_r^3 \tag{13}$$

2.2. Temperature and Saturation Effects

Temperature Effects

Both stator and rotor resistances increase with temperature. The stator temperature can be monitored and approximate correction factor can be applied, but there is no easy way to measure or estimate the rotor temperature. Precise prediction of temperature in each part of the machine requires detailed dynamic thermal model that depends on machine geometry, material characteristics, cooling effects, etc, and is extremely difficult to estimate. The machine transient thermal response can be given approximately by a first order model where the temperature rise ΔT can be given as

$$\Delta T = \frac{P_{tl}}{\theta\ (1 + \tau\ s)} \tag{14}$$

where P_{tl} = total machine loss, θ = steady state thermal resistance and τ = thermal time constant. The θ and τ parameters can be estimated approximately by experimentation. Both rotor and stator resistances can be corrected for temperature effects by using the well known formula:

$$R_{T2} = R_{T1}\ (1 + \alpha_{T1}\ (T_2 - T_1)) \tag{15}$$

where α_{T1} = temperature coefficient (usually at T_1=25 °C), and $\Delta T = (T_2 - T_1)$. The temperature corrected resistances are then used to calculate fundamental and harmonic copper losses. For harmonic rotor losses, the skin effect is superimposed on the temperature effect.

Saturation effects

Although saturation is strictly present in both leakage and magnetizing inductances, we will ignore saturation in the former and represent magnetizing inductance L_m saturation by a piece-wise linear function of magnetizing current I_m:

$$\begin{aligned} L_m &= L_{mo} && ,if\ I_m < I_{mo} \\ &= L_{mo} - m\,(I_m - I_{mo}) && ,if\ I_m > I_{mo} \end{aligned} \qquad (16)$$

where L_{mo} = unsaturated inductance and I_m = magnetizing current at the start of saturation. The saturation coefficient m is selected to best fit the actual saturation curve of the machine.

2.3. Per-Phase Harmonic Equivalent Circuit

The effects of time harmonics have been traditionally investigated by solving the per-phase equivalent circuit [1] shown in Fig. 2(a), where the harmonic stray losses are represented by shunt resistances (R_{ssn} and R_{rsn}). For each harmonic component, the circuit is solved and superposition principle is applied to get the overall harmonic effect [1]. In this way, the frequency dependence of machine parameters can be taken into account precisely. The following simplifying assumptions can be made at this point:

. For sinusoidal PWM or hysteresis-band current-controlled inverter, only the carrier frequency can be considered for computation of frequency dependent parameters, and the resulting circuit can be used to compute the effect of all the harmonics with little loss of precision.

. The harmonic frequencies are sufficiently high such that the harmonic slip s_n is essentially one.

With these assumptions, Fig 2(a) can be converted to series equivalent form of Fig. 2(b). The barred parameters are simply the series equivalents of the corresponding original parameters. For example, the series equivalent stator stray loss resistance can be expressed as

$$\bar{R}_{ssn} = \frac{R_{ssn} X_{ssn}^2}{R_{ssn}^2 + (X_{ssn} + X_{lsn})^2} \approx \frac{R_{ssn} X_{ssn}^2}{R_{ssn}^2 + X_{lsn}^2} \qquad (17)$$

since the secondary leakage reactance X_{ssn} is very small. The harmonic rotor resistance R_m is shown split into fundamental rotor resistance R_r and $(R_m - R_r)$ Similarly, R_{ssn} is shown as the sum of the fundamental frequency stray loss resistance R_{s11} and $(R_{ssn} - R_{s11})$ The harmonic core loss resistance R_{mn} is substituted in Fig. 2(b) by a series combination of the fundamental core loss resistance R_m and a modified secondary magnetizing reactance X_{lmn}', so as to ensure constancy of harmonic core loss P_{cln}. From Fig. 2(a), the harmonic core loss P_{cln} (neglecting small X_{lmn} is given as

$$P_{cln} = \frac{3 V_{mn}^2}{R_{mn}} \qquad (18)$$

where V_{mn} is the rms harmonic airgap voltage. From Fig. 2(b), P_{cln} is given by

$$P_{cln} = \frac{3 V_{mn}^2 R_m}{R_m^2 + X_{lmn}'^2} \qquad (19)$$

In order to keep the harmonic core loss invariant, the two equations must yield the same result. By equating the two expressions, the modified secondary magnetizing reactance is derived as follows:

$$X_{lmn}' = \sqrt{R_{mn} R_m - R_m^2} \qquad (20)$$

The circuit of Fig. 2(b) is next transformed into the modified "shunt" form of Fig. 2(c). The final values of the harmonic stray loss resistances R_{ssn}' and R_{rsn}' are obtained by equating the corresponding resistive terms in Figs. 2(b) and 2(c). Neglecting the small X_{rsn}' the following expression is obtained:

$$\frac{R_{rsn}' X_{lrn}}{R_{rsn}'^2 + X_{lrn}^2} = R_{rle} \qquad (21)$$

where $R_{rle} = R_{rsn} + (R_m - R_r)$. Solving for R_{rsn}',

$$R_{rsn}' = \frac{X_{lrn}^2 \pm \sqrt{\left(\frac{X_{lrn}^2}{R_{rle}}\right)^2 - 4 X_{lrn}^2}}{2} \qquad (22)$$

For most practical drives, $R_{rsn} > X_{lrn}$ and therefore, the plus sign is considered in the above equation. With a similar procedure, the expression of R_{ssn}' can be derived. In practice, the value of R_{s11} is very small compared to R_{ssn}. Therefore, R_{ssn}' can be taken equal to R_{ssn}. Note that R_{rsn}' represents not only the rotor harmonic stray loss, but also the additional harmonic copper loss due to skin effect.

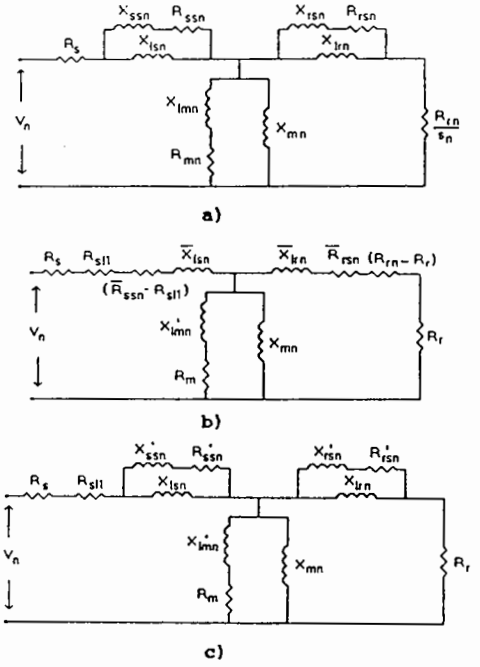

Fig. 2. Per phase harmonic equivalent circuit of induction motor.
(a) Generic circuit for harmonic of order n.
(b) "Series" equivalent form of circuit (a).
(c) Modified "shunt" equivalent form of circuit (b).

2.4. Equivalent Circuit Derivation in Synchronously Rotating Frame

The per-phase equivalent circuit derived in Fig. 2(c) is only valid for steady state operation, and can not be used for dynamic performance study. Usually, synchronously rotating frame D^e-Q^e equivalent circuits [12] are used for dynamic study. The standard D^e-Q^e equivalent circuits can not be represented with core loss resistor in parallel with magnetizing inductance because dc current (equivalent fundamental frequency current) will not flow through it. In this section, these circuits will be modified to incorporate core loss resistor, and then the harmonic equivalent circuits will be superimposed to derive the unified lossy equivalent circuits.

D^e-Q^e Equivalent Circuits with Core Loss Resistor

The stationary frame D^s-Q^s equivalent circuits [12] can easily incorporate core loss resistor in parallel with magnetizing inductance. With this modifications the following equations can be written easily

$$R_s \begin{pmatrix} i_{qs}^s \\ i_{ds}^s \end{pmatrix} + L_{ls} \frac{d}{dt} \begin{pmatrix} i_{qs}^s \\ i_{ds}^s \end{pmatrix} + R_m \begin{pmatrix} i_{qrm}^s \\ i_{drm}^s \end{pmatrix} = \begin{pmatrix} v_{qs}^s \\ v_{ds}^s \end{pmatrix} \qquad (23)$$

$$-L_m \frac{d}{dt}\begin{pmatrix} i^s_{qm} \\ i^s_{dm} \end{pmatrix} + R_m \begin{pmatrix} i^s_{qrm} \\ i^s_{drm} \end{pmatrix} = \begin{pmatrix} 0 \\ 0 \end{pmatrix} \quad (24)$$

$$-\omega_r \begin{pmatrix} \Psi^s_{dr} \\ \Psi^s_{qr} \end{pmatrix} + R_r \begin{pmatrix} i^s_{qr} \\ i^s_{dr} \end{pmatrix} + L_{lr} \frac{d}{dt}\begin{pmatrix} i^s_{qr} \\ i^s_{dr} \end{pmatrix} + L_m \frac{d}{dt}\begin{pmatrix} i^s_{qm} \\ i^s_{dm} \end{pmatrix} = \begin{pmatrix} v^s_{qr} \\ v^s_{dr} \end{pmatrix} \quad (25)$$

These stationary frame equations can now be converted to synchronously rotating frame by multiplying each term with transformation matrix to result the following equations

$$R_s \begin{pmatrix} i_{qs} \\ i_{ds} \end{pmatrix} + \omega_e \begin{pmatrix} \Psi_{dls} \\ -\Psi_{qls} \end{pmatrix} + L_{ls} \frac{d}{dt}\begin{pmatrix} i_{qs} \\ i_{ds} \end{pmatrix} + R_m \begin{pmatrix} i_{qrm} \\ i_{drm} \end{pmatrix} = \begin{pmatrix} v_{qs} \\ v_{ds} \end{pmatrix} \quad (26)$$

$$\omega_e \begin{pmatrix} \Psi_{dm} \\ \Psi_{qm} \end{pmatrix} + L_m \frac{d}{dt}\begin{pmatrix} i_{qm} \\ i_{dm} \end{pmatrix} - R_m \begin{pmatrix} i_{qrm} \\ i_{drm} \end{pmatrix} = \begin{pmatrix} 0 \\ 0 \end{pmatrix} \quad (27)$$

$$(\omega_e - \omega_r) \begin{pmatrix} \Psi_{dr} \\ \Psi_{qr} \end{pmatrix} + R_r \begin{pmatrix} i_{qr} \\ i_{dr} \end{pmatrix} + L_{lr} \frac{d}{dt}\begin{pmatrix} i_{qr} \\ i_{dr} \end{pmatrix} + L_m \frac{d}{dt}\begin{pmatrix} i_{qm} \\ i_{dm} \end{pmatrix} = \begin{pmatrix} v_{qr} \\ v_{dr} \end{pmatrix} \quad (28)$$

Note that the terms $\omega_e \psi_{dm}$, $\omega_e \Psi_{dls}$, etc, represent the speed voltages due to rotation of reference axes. The eqns. 26 - 28 can be represented by equivalent circuits shown in Fig. 3 (exclude the branches enclosed in dashed lines).

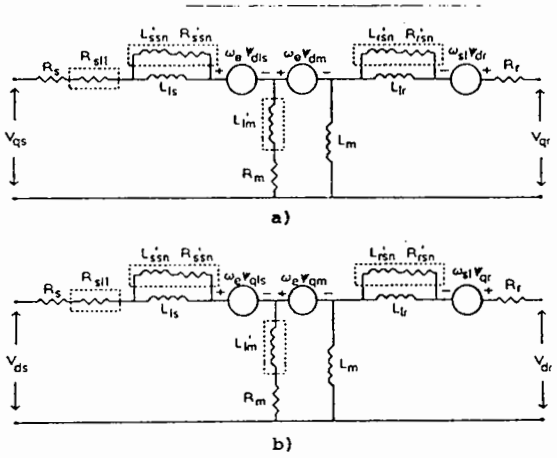

Fig. 3. Lossy D-Q equivalent circuits in synchronously rotating reference frame.
(a) Q - axis circuit. (b) D - axis circuit.

D^e-Q^e Equivalent Circuits with Core Loss and Harmonic Loss

Although the harmonic equivalent circuit of Fig. 2(c) is a per phase stationary frame circuit, it can be used in the synchronously rotating frame as well, with little loss of precision because the axes rotation will have the effect of adding (or subtracting) the fundamental frequency to the particular harmonic frequency. Therefore, under the assumption $f_n >> f$, the effect of axes rotation is negligible. The circuit of Fig. 2(c) can therefore, be superimposed on the synchronously rotating frame D^e-Q^e equivalent circuits with core loss resistance, resulting in the complete lossy dynamic D^e-Q^e equivalent circuits shown in Fig. 3. The model represents true physical behavior of the machine, and can be used for lossy dynamic D^e-Q^e equivalent circuits shown in Fig. 3. The model represents true physical behavior of the machine, and can be used for evaluation of fundamental and harmonic losses, as well as for dynamic studies. Since at steady state conditions all fundamental variables appear as dc quantities, the fundamental current will not flow through R'_{ssn} and R'_{rsn}, i.e., the harmonic stray loss shunt terms have no effect on fundamental losses. Similarly, the presence of the secondary magnetizing inductance L'_{lm} has no effect on fundamental core loss. For harmonic losses, the circuits of Fig. 3 give almost the same result as that of Fig. 2(c). This follows from the fact that the harmonic fluxes are very small and the corresponding harmonic voltages present in the dependent voltage sources are negligible, i.e., the terms such as $\omega_e \psi_{dm}$ essentially represent fundamental counter emf. During transient operations some amount of fundamental current will flow through the shunt stray loss resistances, and this is theoretically coherent, because a change in fundamental leakage flux induces extra stray losses both in the stator and the rotor. During the transient, the effective rotor resistance seen by the fundamental current increases and the effective inductance decreases, and this is also consistent with the theory, because the skin effect is present during sinusoidal transients.

In order to use the equivalent circuits of Fig. 3, it is necessary to evaluate the parameters for the particular machine. The fundamental frequency parameters can be easily obtained from standard tests, but harmonic frequency parameters are much more difficult to obtain experimentally [4]. On the other hand, accurate theoretical prediction of harmonic frequency parameters also constitutes a formidable task. In this project, the standard fundamental frequency parameters are taken from literature [15], and the remaining parameters are estimated from practical considerations [7] (see Table 1).

Table 1. Power circuit parameters of the drive system

Machine: 10 hp 230 / 460 V 27/13.5 A
1755 rpm 60 Hz Class B 1.15 SF

D^e-Q^e equivalent circuit parameters

R_s=0.2264 Ω	R_r=0.1256 Ω	R_m=129.06 Ω
L_{ls}=0.00155 H	L_{lr}=0.00193 H	L_m=0.0275 H
R_{sll}=0.0341 Ω	R_{ssn}'=146.52 Ω	R_{rsn}'=169.63 Ω
L_{lm}'=0.0032 H	L_{ssn}=7.75 10^{-5} H	L_{rsn}=9.65 10^{-5} H

Diode: POWEREX CD 411230 Dual diode module
30 A / 1200 V
Drop equation parameters:
v_{d0}=0.8 V K=0.052 m=0.585

Transistor: POWEREX KS 524503 Single Darlington transistor module, 30 A / 600 V
Drop equation parameters:
v_{t0}=0.7 V R_t=0.020

3. LOSS MODELING OF CONVERTER SYSTEM

3.1. Loss Modeling of Diode Rectifier

For a diode rectifier, the switching loss can be neglected and only the conduction loss need to be considered. Fig. 4 shows the proposed equivalent circuit for the diode rectifier, where V_r = ideal rectifier voltage profile and the dc link inductance is $L_d = 2 L_s$, where L_s = per-phase source leakage inductance. The two conducting diodes can be modeled by an off-set voltage V_f in series with a nonlinear resistance R as indicated. From the conduction characteristics of a particular diode, the voltage drop equation can be derived by using the software TABLE-CURVE [13]. The software takes a set of (x,y) coordinate pairs as input and calculates the equation of the best fitting curve as follows:

$$v_{dd} = v_{do} + K i_d^m \quad (29)$$

where v_{do} = offset voltage and m = resistive drop exponent. The instantaneous conduction loss P_{ild} for the diode bridge can then be given as

$$P_{dd} = 2 v_{dd} i_1 \quad (30)$$

3.2. Loss Modeling of PWM Inverter

For a PWM inverter both conduction and switching losses should be considered.

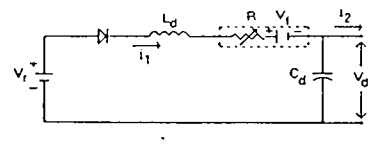

Fig. 4. Diode rectifier equivalent circuit.

Conduction Loss

The conduction loss in the inverter is distributed between transistors and feedback diodes. Fig. 5(a) shows an inverter phase leg with feedback diodes and snubbers, and Fig. 5(b) shows its conduction loss equivalent circuit. Again, from the transistor saturation characteristics, the following linear voltage drop equation can be derived with the help of TABLE-CURVE:

$$v_{td} = v_{t0} + R_t i_c \tag{31}$$

For the feedback diodes, the voltage drop eqn. 29 is valid for the particular devices.

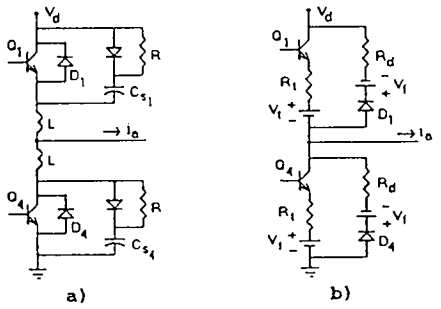

Fig. 5. (a) Transistor inverter phase leg.
(b) Conduction loss equivalent circuit of inverter phase leg.

Switching Loss

Fig. 6 shows the typical turn-on and turn-off switching waves for transistor Q_1 of Fig. 5. Evidently, the snubber power loss of the inverter is given as

$$P_s = (3/2) N_s C_s V_d^2 f \tag{32}$$

where N_s = the number of switchings (ON-OFF or OFF-ON) in a phase leg, per cycle of fundamental frequency f, V_d= dc link voltage and C_s = snubber capacitance. The snubber loss can be represented by an equivalent shunt resistance R_s across the dc bus as follows:

$$R_s = \frac{2}{3 f N_s C_s} \tag{33}$$

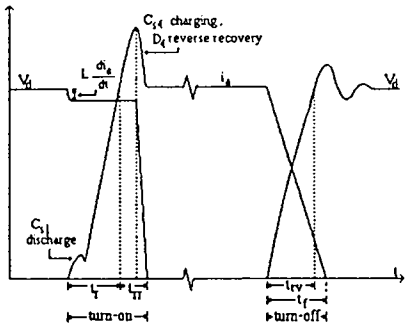

Fig. 6. Typical turn-on and turn-off switching waves for transistor Q_1 in the phase leg (Fig. 5).

Turn-off Switching Loss

Turn-off and turn-on switching losses have been discussed and mathematically analyzed in detail by Mc Murray [8] for a dc chopper. The same mathematical analysis can be easily extended to inverter design. It can be shown [8] [14] that for optimum total loss (snubber loss + turn-loss) , usually the value of C_s is small such that the collector-emitter voltage v_{cc} rise time t_{rv} is smaller than the colector current i_c fall time t_f. In this condition, it can be shown that

$$t_{rv} = \sqrt{\frac{2 C_s V_d t_f}{I_{av}}} \tag{34}$$

where V_d = dc link voltage, and I_{av} = half-cycle average of absolute value of load current. Therefore, the average transistor turn-off power loss P_{toff} can be derived as

$$P_{toff} = 3 K_{off} V_d (N_s/2) I_{av} f = \frac{V_d^2}{R_{toff}} \tag{35}$$

where $N_s/2$ = number of lossy turn-offs per converter leg in one cycle of fundamental frequency f, and the turn-off constant K_{off} is given by:

$$K_{off} = \frac{t_f}{2}\left(1 - \frac{4}{3}\frac{t_{rv}}{t_f} + \frac{1}{2}\left(\frac{t_{rv}}{t_f}\right)^2\right) \tag{36}$$

The eqns. 35 and 36 indicate that the turn-off loss decreases as the snubber capacitance is increased. The transistor turn-off loss of eqn. 36 can be represented by an equivalent dc link shunt resistance as

$$R_{toff} = \frac{V_d}{3 K_{off} (N_s/2) I_{av} f} \tag{37}$$

Turn-on Switching Loss

For a transistor inverter, no snubber inductance L as indicated in Fig. 5 is normally used. The stray inductance due to the wiring between the dc link capacitor and the transistor will act as a parasitic inductance for turn-on snubber. Using a procedure similar to that used for turn-off loss computation, the transistor turn-on power loss can be given as [8]

$$P_{ton} = 3 K_{on} V_d (N_s/2) I_{av} f = \frac{V_d^2}{R_{ton}} \tag{38}$$

where the turn-on constant K_{on} is defined as

$$K_{on} = \frac{t_{fv}}{2}\left(1 - \frac{4}{3}\frac{t_r}{t_{fv}} + \frac{1}{2}\left(\frac{t_r}{t_{fv}}\right)^2\right) \tag{39}$$

where t_r = colector current i_c rise time and $t_{fv} = t_r + t_{rr}$ is the v_{cc} voltage fall time. Again, t_r is given by the expression

$$t_r = \sqrt{\frac{2 L t_{fv} I_{av}}{V_d}} \tag{40}$$

From eqn. 38, the transistor turn-on loss can be represented by an equivalent dc link shunt resistance as

$$R_{ton} = \frac{V_d}{3 K_{on} (N_s/2) I_{av} f} \tag{41}$$

The eqns. 38-40 indicate that the turn-on loss decreases as the inductance L is increased.

4. SIMULATION STUDY

Both the converter and machine models, as discussed above, were simulated in detail (using PC-SIMNON language) for a 10 HP drive with indirect vector control. The inverter uses hysteresis-band current control where the number of switchings per cycle N_s and the carrier frequency f_c are counted. These variables are then used in the computation of converter and machine frequency dependent parameters. The equivalent circuits of Fig. 3 are used in the derivation of machine state equations. Both steady state and transient conditions of the system were considered in the validation process of the models. Table 1 shows the complete power circuit parameters of the drive. The steady state system performance was initially investigated, for various load torque and speed conditions. Fig. 7 shows the machine loss at various load torque and speed. For a given speed, the total loss increases with torque, primarily due to increased fundamental copper and stray load losses. For a constant load torque, the losses increase with speed mainly because of additional core loss and friction and windage losses. Fig. 8 shows the corresponding total converter loss for the same load torque and speed conditions. It can be seen that the converter loss is more affected by an increase in load torque at constant speed, rather than by increase of machine speed at constant load torque. This can be explained as follows:
With rated flux, the machine current is essentially a function of load torque and is practically independent of speed. Therefore, the inverter losses that basically depend on machine current, is dominantly influenced by load torque. Again, the diode rectifier loss is a function of dc link current that increases with converter output power Therefore, the rectifier loss is influenced by both speed and torque of the machine. Fig. 9 shows the total system efficiency at various torque and speed conditions.

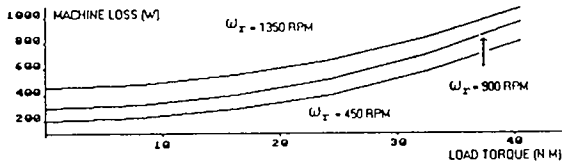

Fig. 7. Machine loss at various torque and speed

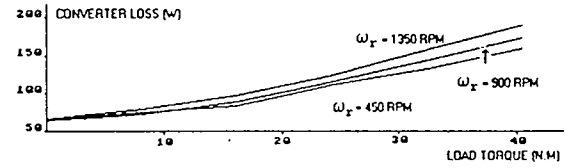

Fig. 8. Converter loss at various torque and speed.

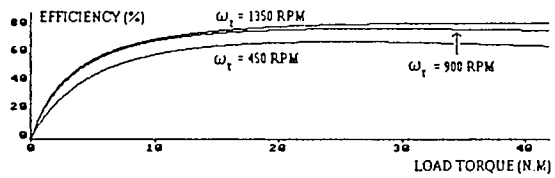

Fig. 9. System efficiency at various torque and speed.

Finally, the transient torque response of the vector-controlled drive is investigated at constant speed, as indicated in Fig. 10, to study possible effect for D^e-Q^e equivalent circuits modification. Fig. 10(a) shows the step in the torque component of current (i_{qs}^*) at the rated flux condition. Fig. 10(b) shows the corresponding torque response for lossless converter and ideal D^e-Q^e machine model with slip gain parameter tuned with the nominal machine parameters. The observed rise time is essentially due to intrinsic delay of hysteresis-band current controller. Fig. 10(c) shows the response for lossy converter-machine model with nominal parameter slip gain tuning, and Fig. 10(d) is for the same model except the slip gain is tuned for actual machine parameters at the operating condition. It appears that the response for all the three conditions are practically identical.

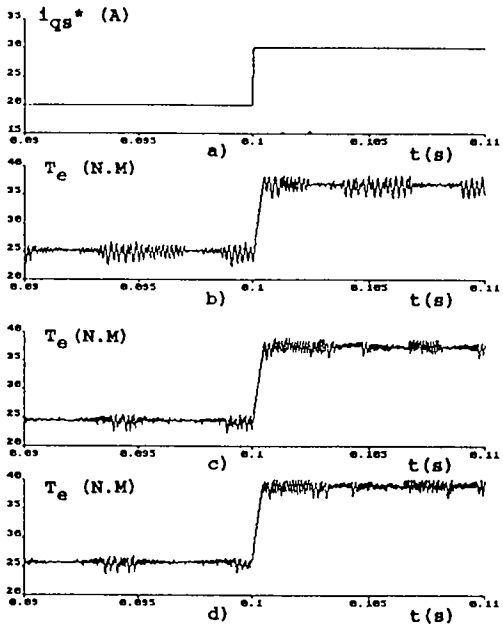

Fig. 10. Torque response of the drive at rated flux (speed=900 rpm)
(a) Command current step.
(b) Ideal and lossless converter-machine model (slip gain parameters are nominal machine parameters).
(c) Lossy converter-machine model (slip gain parameters are nominal machine parameters).
(d) Lossy converter-machine model (slip gain parameters track with machine parameters)

5. CONCLUSION

In this paper, a unified loss model of converter induction machine system has been developed such that it truly represents the physical system. Therefore, the model can be used for precise performance investigation under both static and dynamic conditions. The model incorporates all the relevant losses, and takes into account the effects of temperature and saturation on the induction machine performance The simulation study confirmed the validity of the model for both steady state and dynamic conditions. Although the basic motivation for the project was to predict the losses in a vector-controlled induction motor drive that uses fuzzy logic based efficiency optimization control, it can also be used for other purposes, such as loss-optimized design of converter machine system, loss evaluation of a PWM algorithm, cooling system design, and general dynamic performance studies.

6. ACKNOWLEDGMENT

The authors wish to acknowledge the help of Marcelo G. Simoes and Sunil M. Chhaya in this project.

7. REFERENCES

[1] V. B. Honsinger, "Induction motors operating from inverters", IEEE IAS Annual Meeting Conf. Rec., pp. 1276-1285, 1980.

[2] B. J. Chalmers and B. R. Sarkar, "Induction motor losses due to nonsinusoidal supply waveforms", Proc. IEEE vol. 115, pp.1777-1782, Dec. 1968.

[3] M. R. Udayagiri and T. A. Lipo, "Simulation of inverter fed induction motors including core losses", IEEE IECON'89 Conf. Rec., pp. 232-237, 1989.

[4] D. W. Novotny et al., "Frequency dependency of time harmonic losses in induction machines", Int'l Conf. on Elec. Machines Conf. Rec., pp. 233-238, 1990.

[5] F. G. de Buck et al., "A simple but reliable loss model for inverter supplied induction motors", IEEE Trans. Ind. Appl., vol. 20, pp. 1190-1202, Jan./Feb. 1984.

[6] E. A. Klingshirn and H. E. Jordan, "Polyphase induction motor performance and losses on nonsinusoidal voltage sources", IEEE Summer Power Meeting Conf. Rec., Portland, Oregon, pp. 624-631, 1967.

[7] K. Kawagishi et al., "Frequency dependency of induction motor parameters and their measuring method", Int'l. Pow. Elec. Conf. Rec., Tokyo, pp. 202-213, 1983.

[8] W. McMurray, "Selection of snubbers and clamps to optimize the design of transistor switching converters", IEEE Trans Ind. Appl., vol. 16, pp. 513-523, July/Aug. 1980.

[9] M. M. Jovanovic et al., "Characterization of high power BJT's for motor drive applications", IEEE IAS Annul Meet. Conf. Rec., pp. 440-447, 1986.

[10] Y. Ikeda et al., "The power loss of a PWM voltage-fed inverter", PESC Conf. Rec., pp. 277-283, 1988.

[11] P. L. Alger et al., "Stray load losses in polyphase induction machines", AIEE Trans. on Pow. App. and Syst., vol. 78, pp. 349-357, 1959.

[12] B. K. Bose, Power Electronics and AC Drives, Prentice Hall, NJ, 1986.

[13] TableCurve 3.0 User's Manual, Jandel Scientific, CA, 1991.

[14] B. W. Williams, Power Electronics, John Wiley, NY, 1987.

[15] J. J. Cathey , and P. Famouri, "Loss minimization control of an induction motor drive", IEEE Ind. Appl. Soc. Trans., Jan-Feb, 1991, Vol. 27, no. 1, pp 32-37.

NRMRL-RTP-P-185

TECHNICAL REPORT DATA
(Please read Instructions on the reverse before completing)

1. REPORT NO.	2.	3. RECI
EPA/600/A-97/022		

4. TITLE AND SUBTITLE
Loss Modeling of Converter Induction Machine System for Variable Speed Drive

5. REPORT DATE

6. PERFORMING ORGANIZATION CODE

7. AUTHOR(S) G. C. D. Sousa and B. K. Bose (Univ. of Tenn.) J. Cleland (RTI), and R. Spiegel and J. Chappell (EPA)

8. PERFORMING ORGANIZATION REPORT NO.

9. PERFORMING ORGANIZATION NAME AND ADDRESS
Dept. of Electrical Engrg. Research Triangle Inst.
The Univ. of Tennessee PO Box 12194
Knoxville, TN 37996 Rsrch Tri. Pk, NC 27709

10. PROGRAM ELEMENT NO.

11. CONTRACT/GRANT NO.
CR 818282 (RTI)

12. SPONSORING AGENCY NAME AND ADDRESS
EPA, Office of Research and Development
Air Pollution Prevention and Control Division
Research Triangle Park, NC 27711

13. TYPE OF REPORT AND PERIOD COVERED
Published paper; 9/91-4/96

14. SPONSORING AGENCY CODE
EPA/600/13

15. SUPPLEMENTARY NOTES APPCD project officer is Ronald J. Spiegel, Mail Drop 63, 919/541-7542. Presented at IEEE Int. Conf. on Industrial Electronics, Control, Instrumentation and Automation, San Diego, CA, 11/9-13/92.

16. ABSTRACT The paper describes a unified loss model development of a converter machine system such that steady state loss characteristics and the dynamic behavior of both machine and converter are accurately represented in the model. (NOTE: A reliable and reasonably accurate loss model of a converter induction machine system is extremely important for performance prediction of variable speed drive.) Machine electrical losses (e.g., stator and rotor copper loss, core loss, and stray loss) are considered for both fundamental and harmonic frequencies. Also considered are the skin effect on rotor resistance, temperature effect on both stator and rotor resistances, magnetizing inductance saturation, and friction and windage loss. All the above features are incorporated in synchronously totating frame dynamic D-Q equivalent circuits. A converter system that includes a diode rectifier and pulse width modulated (PWM) transistor inverter has been modeled accurately for conduction and switching losses. The machine and converter models have been simulated for a vector controlled drive system, and validity in both steady state and transient conditions has been verified. The models are valid for any type of control strategy with an arbitrary PWM algorithm.

17. KEY WORDS AND DOCUMENT ANALYSIS

a. DESCRIPTORS	b. IDENTIFIERS/OPEN ENDED TERMS	c. COSATI Field/Group
Pollution	Pollution Prevention	13B
Variable Speed Drives	Stationary Sources	13I
Induction Motors	Loss Modeling	09C
Electric Converters	Electrical Losses	09E

18. DISTRIBUTION STATEMENT	19. SECURITY CLASS *(This Report)*	21. NO. OF PAGES
Release to Public	**Unclassified**	
	20. SECURITY CLASS *(This page)* **Unclassified**	22. PRICE

EPA Form 2220-1 (9-73)